Journal of Applied Physics

A theory of contact resistance under AC conditions

Cite as: J. Appl. Phys. 127, 125107 (2020); https://doi.org/10.1063/1.5142511
Submitted: 13 December 2019 . Accepted: 29 February 2020 . Published Online: 24 March 2020

Foivos Antoulinakis, and Y. Y. Lau

View Online

Export Citation

CrossMark

ARTICLES YOU MAY BE INTERESTED IN

Charge carrier trapping by dislocations in single crystal diamond
Journal of Applied Physics 127, 125102 (2020); https://doi.org/10.1063/1.5140662

Acoustic computational metamaterials for dispersion Fourier transform in time domain
Journal of Applied Physics 127, 123101 (2020); https://doi.org/10.1063/1.5141057

Theoretical calculations of the mean escape depth of secondary electron emission from compound semiconductor materials
Journal of Applied Physics 127, 125304 (2020); https://doi.org/10.1063/1.5144721

Challenge us.
What are your needs for periodic signal detection?

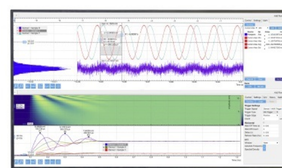

Zurich Instruments

© 2020 Author(s).

Journal of Applied Physics ARTICLE scitation.org/journal/jap

A theory of contact resistance under AC conditions

Cite as: J. Appl. Phys. **127**, 125107 (2020); doi: 10.1063/1.5142511
Submitted: 13 December 2019 · Accepted: 29 February 2020 ·
Published Online: 24 March 2020

Foivos Antoulinakis and Y. Y. Lau[a)]

AFFILIATIONS

Department of Nuclear Engineering and Radiological Sciences, University of Michigan, Ann Arbor, Michigan 48109, USA

[a)]**Author to whom correspondence should be addressed:** yylau@umich.edu

ABSTRACT

Electrical contact is an important issue to high power microwave sources, pulsed power systems, field emitters, thin film devices and integrated circuits, interconnects, etc. Contact resistance and the enhanced ohmic heating that results have been treated mostly under steady state (DC) condition. In this paper, we consider the AC contact resistance for a simple geometry, namely, that of two semi-infinite slab conductors of different thicknesses joined at $z = 0$, with current flowing in the z-direction. The conductivity of the two planar slabs may assume different values. We propose a procedure to accurately calculate the normalized contact resistance under the assumption $\sigma \gg \omega\epsilon$, where ω is the frequency, σ is the electrical conductivity, and ϵ is the dielectric constant of the material in either channel. We found that in the low frequency limit, the normalized AC contact resistance reduces to the DC case, which was solved exactly by Zhang and Lau. At very high frequency, we found that the normalized contact resistance is proportional to $\sqrt{\omega}$, in which case the resistive skin depth becomes the effective channel width, and the physical origin of the contact resistance is identified. The transition between the high and low frequency limits was explored, where, in some cases, the normalized contact resistance may become negative, meaning that the total resistance is less than the total bulk resistance expected from the two current channels. In other cases, the numerical data suggest that the normalized contact resistance is proportional to ω in the transition region. Other issues are addressed.

Published under license by AIP Publishing. https://doi.org/10.1063/1.5142511

I. INTRODUCTION

Contact problems account for 40% of all electrical/electronic failures, ranging from small scale consumer electronic devices to large scale military and aerospace systems.[1–3] In pulsed power systems and high power microwave sources, poor electrical contact prevents efficient power coupling to the load,[4] produces unwanted plasma,[5] and even damages the electrodes. On the largest scales, faulty electrical contact has caused failure of the Large Hadron Collider and similarly threatens the International Thermonuclear Experimental Reactor.[6] On the smallest scales, electrical contact and local heating are very important issues in microelectronics,[7,8] integrated circuits,[8] thin film devices,[9] carbon nanotube[10] and carbon nanofiber based cathodes[11] and interconnects,[8,12] field emitters,[13] thin film-to-bulk contacts,[14–17] semiconductor nanolasers,[18,19] and ultrafast and nanoscale diodes.[20–22]

The quality of a contact is often measured by the contact resistance.[1,2] Despite its importance, contact resistance and the enhanced ohmic heating that results have been treated mostly under steady state (DC) condition.[1,2,23–29] The evaluation of contact resistance in the AC case is significantly more complex than the DC case. New features, such as the resistive skin effect and inductive and capacitive effects, as well as radiation losses, are totally absent in a DC theory. For the AC case, the simple "a-spot" geometry has received some attention.[25,30–32] The a-spot geometry refers to two current channels, made of the same materials, joined with each other only through a circular hole of radius a.[1,2] A statistical theory for a collection of asperities at the interface of two conductors under AC condition was given by Tang *et al.*,[33] who ignored the all-important skin effects and the effects of dissimilar materials.

We have initiated a theoretical study of AC electrical contact using the Cartesian geometry shown in Fig. 1, allowing for contacts between dissimilar materials. An AC current of frequency ω is launched from the left channel at a large negative value of z, and it exits at the right channel at a large positive value of z. The dimensions and the electrical properties (permittivity ε, conductivity σ, and permeability μ, all assumed real) are specified in Fig. 1. The two conducting channels, with an interface at $z = 0$, are surrounded by vacuum. We have formulated the boundary value problem for Fig. 1 which satisfies the Maxwell equations in the various regions, interior and exterior to the current channel. In this paper, we shall restrict our discussion to the study of resistive loss at the contact in the regime $\sigma \gg \omega\varepsilon$ for both conducting channels. Under this assumption, we found that the current flow pattern within the

Published under license by AIP Publishing.

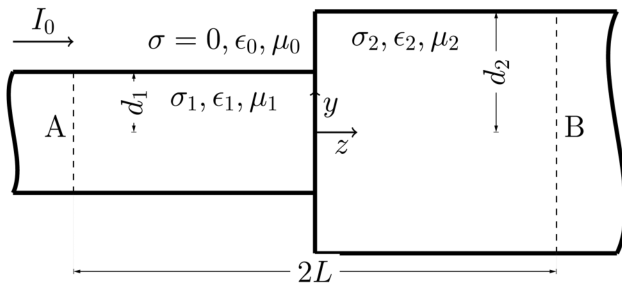

FIG. 1. Two Cartesian current channels, each with length L and joint at $z = 0$, are surrounded by vacuum. An AC current of the form $I_0 e^{-i\omega t}$ enters the left surface A and exits the right surface B.

current channel is essentially unaffected by the solution in the vacuum region, just like the DC case. We should stress that our solutions using this simplifying assumption have been spot-checked against the complete electromagnetic field solutions that we have constructed for all regions, both exterior and interior to the channel. We shall further comment on the general case in Sec. IV.

The two-dimensional, planar, model (Fig. 1) gives considerable physical insight into the nature of current crowding from DC to high-frequency conditions. Similar to the DC case,[24] we expect the qualitative features to hold for the cylindrical geometry. This study also reveals the deleterious effects of conductor misalignment on the contact resistance, especially at high frequencies. Modulation at 10 GHz and beyond is being pursued for nanolight-emitting-diodes for on-chip optical communications,[19] making high-frequency AC contact resistance in that frequency range relevant.

The resistive skin depth $\delta = (2/\omega\mu\sigma)^{1/2}$ in each conducting region is an important length scale. It is frequency dependent. The relative magnitude of δ in the two different regions of the channel and the transverse dimensions of the channels then strongly affect the current flow pattern. Therefore, different scalings for the AC contact resistance are expected for different frequency ranges. This paper reports some such novel scalings. We interpret them by identifying the skin depth as the effective channel widths and then use the corresponding DC scalings.

In Sec. II, we shall first outline the model for the DC contact resistance, concentrating on its salient properties that will be useful in the extension to the AC case, which is described next. In Sec. III, we shall present a few examples of the AC contact resistance, where the novel scalings are presented. The derivation of these novel scalings will be given in Appendixes A–C. Concluding remarks are given in Sec. IV.

II. DEFINITION OF CONTACT RESISTANCE

For the Cartesian geometry shown in Fig. 1, we shall define the contact resistance, first for the DC case and then for the AC case. We assume that, in both cases, there is no variation in the x-direction, and the channel width in the x-direction is W, and that the channel axial length, L, is sufficiently large that the field solutions no longer have any z-variation at $z = \pm L$ for the bulk solution.

A. DC contact resistance

For the DC case, current I_0 with a constant, uniform current density, $I_0/(2Wd_1)$, enters from the left channel at plane A ($z = -L$). This current exits the right channel at plane B ($z = L$) also with a constant, uniform current density, $I_0/(2Wd_2)$. A DC voltage V is needed to drive this current between planes A and B. The total resistance, R, between A and B is then

$$R \equiv \frac{V}{I_0} = \underbrace{\frac{L}{2d_1 W\sigma_1}}_{\text{Bulk}} + \underbrace{\frac{\overline{R_c}}{4\pi W\sigma_2}}_{\text{Interface}} + \underbrace{\frac{L}{2d_2 W\sigma_2}}_{\text{Bulk}}, \tag{1}$$

where the first (last) term on the RHS represents the bulk resistance of the left (right) channel. The middle term of Eq. (1) is defined as the contact resistance, or the interface resistance, which is simply the difference between the total resistance (R) and the bulk resistance of the two current channels. Note that this contact or interface resistance vanishes if $d_1 = d_2$, in which case the DC current flow (and the DC electric field, which is solely in the z-direction) is uniform in both channels, and the channels' bulk resistance, in series, constitutes the total resistance. Thus, the contact or interface resistance in Eq. (1) is also called the spreading resistance (or constriction resistance), as it is a measure of how the current spreads (or constricts) as it approaches and leaves the junction.[1,2,25]

The contact resistance in Eq. (1) is represented by the normalized contact resistance $\overline{R_c}$. It has been computed by Zhang and Lau[24] from their exact electrostatic field solution that satisfies the following boundary conditions (Fig. 1):

$$\sigma_1 E_{z,1} = \sigma_2 E_{z,2}, \quad |y| < d_1, \quad z = 0, \tag{2a}$$

$$E_{y,1} = E_{y,2}, \quad |y| < d_1, \quad z = 0, \tag{2b}$$

$$E_{z,2} = 0, \quad d_1 < |y| < d_2, \quad z = 0, \tag{2c}$$

$$E_{y,1} = 0, \quad |y| = d_1, \quad z < 0, \tag{2d}$$

$$E_{y,2} = 0, \quad |y| = d_2, \quad z > 0. \tag{2e}$$

Equations (2a) and (2b) show, respectively, continuity in the current flow and in the tangential electric field at the channel interface. Equations (2c)–(2e) state that there is no normal electric field at all channel–vacuum interfaces. That is, the conduction current always flows tangentially at the channel–vacuum boundary. It was found[24] that $\overline{R_c}$ depends only on the ratios d_1/d_2 and σ_1/σ_2 (Fig. 1). Accurate scaling laws for $\overline{R_c}$ have been constructed from the numerical solutions of the electrostatic potential for Fig. 1, solved exactly using the boundary conditions (2a)–(2e).[24]

An alternative definition of the contact resistance uses the ohmic power dissipated within the current channel, which can be obtained from the calculated (AC and DC) field solution for Fig. 1. This approach is more suitable for the AC case, in which the "potential" on the surfaces A and B are no longer uniform or

Published under license by AIP Publishing.

constant. For the AC case, the total resistance, R, in the channel may be expressed in terms of the average ohmic power dissipated within the channel,

$$P \equiv \frac{RI_0^2}{2} = \frac{1}{2}\int_{volume} \sigma |E^2| \, dV, \tag{3}$$

where E is the AC electric field over the channel volume, $-L < z < L$. The total resistance R obtained from Eq. (3) is then decomposed into the bulk resistance, R_{b1} and R_{b2}, associated with the channel, and the remainder is then defined as the contact resistance, R_c,

$$R = R_{b1} + R_c + R_{b2}. \tag{4}$$

For the DC case, R_{b1} and R_{b2} are given, respectively, by the first and third term in the RHS of Eq. (1). Comparing R_c, obtained from energy consideration [Eqs. (3) and (4)] and from the published results by Zhang and Lau[24] who used the exact electrostatic field solution without reference to ohmic loss, we obtain an excellent agreement between the two in several test cases.

B. AC contact resistance

For the AC case, the "potential" on the surfaces A and B in Fig. 1 is not defined, and we need to use the power dissipation formulation, Eqs. (3) and (4), for an unambiguous identification of the contact resistance. The conventional definition of potential difference as $\Delta\phi = \int \boldsymbol{E} \cdot \boldsymbol{dl}$ does not work when there are skin effects, since the electric field at $y = 0$ is different than the electric field at $y = d_1$, and, therefore, we would obtain different values for $\Delta\phi$ depending on the path we chose. It is possible to choose any gauge and solve for the potentials in this way, but there are no real benefits in doing so as the resistance will not easily arise from them.

Like the DC case, the power P in Eq. (3) requires the field solution E everywhere within the channel (Fig. 1). However, for the AC case, the boundary conditions to be satisfied need to be modified from Eqs. (2a)–(2e). In general, $E_{\parallel}$ and $(\sigma - i\omega\epsilon)E_{\perp}$ need to be continuous across any boundary. This means that there can now be currents that flow into the conductor from the conductor–vacuum interfaces. This complicates the problem by a significant degree as fields outside the conductors now affect fields inside and, therefore, need to be calculated. However, in this paper, we will focus on good conductors ($\sigma > 10^4$ S/m, ϵ/ϵ_0 of order unity) and frequencies of up to 1 THz. For these values, we get $\omega\epsilon \ll \sigma$ that allows us to ignore the fields in the vacuum once more, like the DC case, and use the same method of series expansion as in Zhang and Lau[24] to obtain the AC solution under the assumption $\omega\epsilon \ll \sigma$. Fields, however, need to satisfy the Helmoltz instead of the Laplace equation, which will result in skin effects for sufficiently high frequencies. Solving for the fields everywhere and accounting for all the boundary conditions properly are possible but doing so only yields an error of up to 0.000 042% in contact resistance when compared to the simplified solution (see Appendix A where the full AC solutions are outlined).

With the assumption $\omega\epsilon \ll \sigma$ on both channels, we may now construct the bulk resistance for the AC case, R_{b1} and R_{b2} in Eq. (4), as follows. First, for large values of $|z|$ (Fig. 1), the AC electric field has only a z-component which is uniform in z but non-uniform in y. It is shown in Appendix B that this bulk solution is given by

$$E_{z,1,b} = \frac{I_0\kappa_1}{2W\sigma_1}\frac{\cos(\kappa_1 y)}{\sin(\kappa_1 d_1)}, \quad E_{z,2,b} = \frac{I_0\kappa_2}{2W\sigma_2}\frac{\cos(\kappa_2 y)}{\sin(\kappa_2 d_2)}, \tag{5}$$

where

$$\kappa_1^2 = \mu_1\epsilon_1\omega^2 + i\omega\mu_1\sigma_1 \cong i\omega\mu_1\sigma_1 \equiv 2i/\delta_1^2, \quad \kappa_2^2 = \mu_2\epsilon_2\omega^2 + i\omega\mu_2\sigma_2 \cong i\omega\mu_2\sigma_2 \equiv 2i/\delta_2^2, \tag{6}$$

which includes the dominant skin effect, i.e., assuming $\sigma_{1,2} \gg \omega\epsilon_{1,2}$. The skin depth for each material is

$$\delta_1 = \sqrt{2/\sigma_1\mu_1\omega}, \quad \delta_2 = \sqrt{2/\sigma_2\mu_2\omega}. \tag{7}$$

Upon using the bulk field solution (5) into the integral (3) for each channel, we find the AC bulk resistance for each channel to be (see Appendix B)

$$R_{b1} = \frac{L}{2W\sigma_1\delta_1}\frac{\sinh\left(\frac{2d_1}{\delta_1}\right) + \sin\left(\frac{2d_1}{\delta_1}\right)}{\cosh\left(\frac{2d_1}{\delta_1}\right) - \cos\left(\frac{2d_1}{\delta_1}\right)}, \quad R_{b2} = \frac{L}{2W\sigma_2\delta_2}\frac{\sinh\left(\frac{2d_2}{\delta_2}\right) + \sin\left(\frac{2d_2}{\delta_2}\right)}{\cosh\left(\frac{2d_2}{\delta_2}\right) - \cos\left(\frac{2d_2}{\delta_2}\right)}, \tag{8}$$

which is to be used in Eq. (4). Note that Eq. (8) reduces to the DC bulk resistance in Eq. (1) in the DC limit $\omega \to 0$ so that $\delta_1 \to \infty$ and $\delta_2 \to \infty$. At high frequencies, $\delta_1 < d_1$ and $\delta_2 < d_2$, Eq. (8) shows that the bulk resistances, R_{b1} and R_{b2}, increase with ω, like $\sqrt{\omega}$.

The total resistance, R, may then be obtained from Eq. (3) after solving for the AC field solution for the entire region, $-L < z < L$ (Fig. 1), and the contact resistance, R_c, may be then obtained by substituting Eq. (8) into Eq. (4). In the numerical examples given in Sec. III, we will again represent this AC contact resistance,

$$R_c = \frac{\overline{R_c}}{4\pi W\sigma_2}, \tag{9}$$

in terms of the normalized resistance $\overline{R_c}$ so that this AC value can immediately be compared with the DC value given in Eq. (1).

Published under license by AIP Publishing.

III. NUMERICAL EXAMPLES OF AC CONTACT RESISTANCE

Numerical examples of the AC contact resistance are presented for three selected cases: (A) $d_1 = d_2$, (B) $d_2 > d_1$, and (C) $d_2 - d_1 \ll d_1$, with $\sigma_1 = \sigma_2$. Case (A) shows the distinct nature of AC contact resistance, as the DC contact resistance equals zero in this case. It also reveals the surprising result that the contact resistance can be negative. Case (B) shows various scalings with frequencies, and Case (C) provides a closer examination of the frequency scaling and offers a quantification of AC contact resistance for slightly uneven surfaces.

A. Case A. $d_1 = d_2 = d$

The setup for this case is shown in Fig. 2. This case is trivial for the DC case in which the contact resistance is zero as the bulk fields are uniform, and, therefore, the sum of the bulk resistance becomes the total resistance. For the AC case, however, the bulk fields shown in Eq. (5) do not satisfy the appropriate boundary conditions for $\sigma_1 \neq \sigma_2$ because of the different skin depths in each material. Without loss of generality we will assume $\sigma_1 > \sigma_2$. By satisfying the boundary conditions on the interface $z = 0$, we can obtain the normalized contact resistance as a function of frequency, as shown in Fig. 3.

There are a few interesting features in Fig. 3. First, for low frequencies, we obtain $\overline{R_c} = 0$. This is because at low frequencies, the skin depth is large, and, therefore, the fields are merely oscillating uniform fields. This was found to be true for $d/\delta_1 < 1$. For high frequencies, we observe a constant contact resistance. This can be explained: at high frequencies, both conductors demonstrate strong skin effects, and we may then take the small skin depths ($\delta_{1,2}$) as the equivalent channel widths ($d_{1,2}$) in a DC case and then use the scaling laws of the DC contact resistance to interpret the numerical results of the AC case. Note that the ratio of the skin depths is constant with frequency and that for the DC case, the contact resistance is only a function of d_2/d_1.[24] Therefore, as we change the frequency, the skin depths also change but not their ratio so the contact resistance is unchanged at high frequencies. This high-frequency constant contact resistance was observed for $d/\delta_2 > 4$. Note that the spreading resistance shown in Fig. 3 approaches a constant at high frequencies, whereas the bulk resistance increases with frequency according to Eq. (8); the relative effect of spreading resistance diminishes at high frequencies. We shall also see in Fig. 11 (in Appendix C) that, in a slightly different context, the spreading resistance also approaches a constant at high frequencies, whereas the bulk resistance increases with frequencies. Constriction resistance at very small skin depths were explored by Zhang *et al.*[25] and Timsit[1] (p. 91).

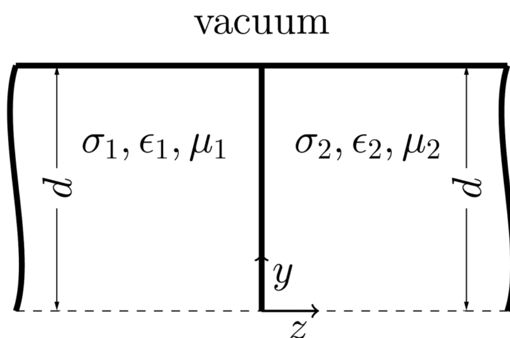

FIG. 2. The setup for $d_1 = d_2 = d$.

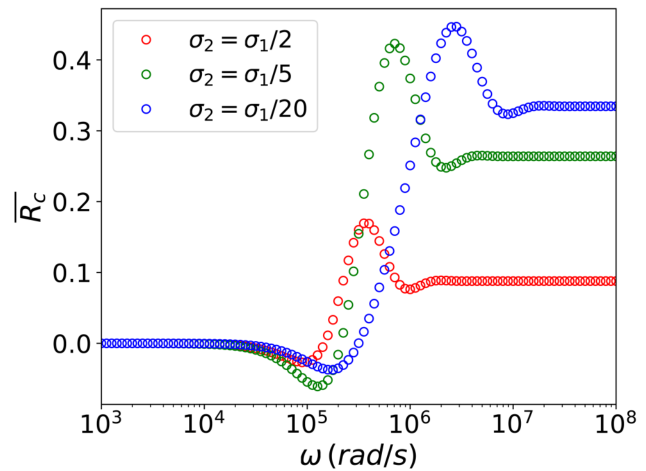

FIG. 3. Normalized contact resistance vs frequency for $d_1 = d_2 = d = 1$ mm and $\sigma_1 = 3.69 \times 10^7$ S/m.

For intermediate frequencies, the contact resistance transitions between the two constant values at low and high frequencies. A further interesting behavior is observed at the lower end of this transition: we obtain $\overline{R_c} < 0$ (Fig. 3). This, of course, does not indicate an overall power gain but a current distribution that is less dissipative compared to the bulk currents. This can be seen in Fig. 4 that shows the current flow pattern when the AC contact resistance is negative (a), zero (b), and positive (c). Figure 4(b) shows zero AC contact resistance, meaning that the total AC resistance in the two conductors happens to be equal to the sum of their respective AC bulk resistance. Compared with Fig. 4(b), Fig. 4(c) [Fig. 4(a)] exhibit more (less) current crowding than Fig. 4(b), and, therefore, its contact resistance is positive (negative) in comparison. That is, Fig. 4(a) [Fig. 4(c)] will produce less (more) electrical heating than that expected from the bulk current of the two conductors. This unexpected reduction in ohmic heating could be exploited in technical applications.

B. Case B. $d_1 < d_2$

This is the more general case. We can numerically solve the boundary conditions (2a)–(2e), assuming the bulk currents in (5) to obtain the remaining fields in both conductors and use those remaining fields to find the normalized AC contact resistance by solving (3) and (4) using (8). Doing so, we obtain $\overline{R_c}$ as a function of ω in Fig. 5.

There are three distinct regions in Fig. 5. For low frequencies, the contact resistance is constant and equal to the DC contact

Published under license by AIP Publishing.

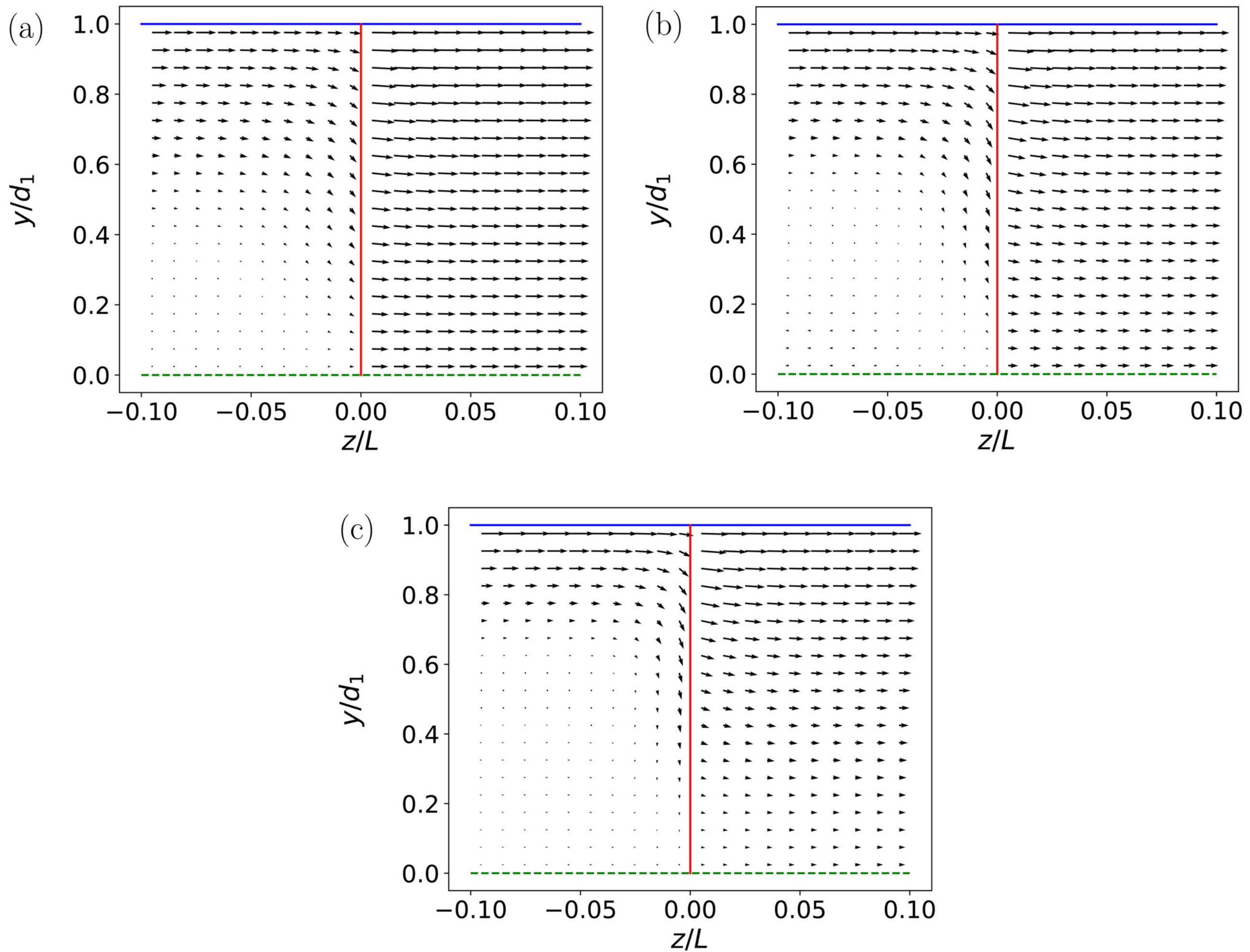

FIG. 4. Current flow patterns for Fig. 2 which show (a) negative ($\omega = 1.33 \times 10^5$ rad/s, $\overline{R_c} = -0.053$), (b) zero ($\omega = 2.66 \times 10^5$ rad/s, $\overline{R_c} = 0$), and (c) positive ($\omega = 5.32 \times 10^5$ rad/s, $\overline{R_c} = 0.228$) AC contact resistance. Here, $d_1 = d_2 = 1$ mm, $\sigma_1 = 10 \times \sigma_2 = 3.69 \times 10^7$ S/m.

resistance.[24] This is because the skin depths are large and the slowly oscillatory fields are basically the uniform DC fields. For high frequencies, we observe $\overline{R_c} \propto \sqrt{\omega}$. To see this, we note that at high frequencies, all currents will be limited to the surface of each conductor because of skin effects. The current profile will resemble Fig. 6. The currents along the top of each conductor are the bulk currents and will not contribute to the contact resistance. The current flowing between points K and M in Fig. 6 will be solely responsible for the dissipative losses that result in contact resistance. In Appendix C, we show that

$$\overline{R_c} = 2\pi \frac{d_2 - d_1}{\delta_2} \propto \sqrt{\omega}. \quad (10)$$

For intermediate frequencies, the contact resistance transitions between the two asymptotes (Fig. 5).

C. Case C. $d_2 - d_1 \ll d_1$, $\sigma_1 = \sigma_2 = \sigma$

This case represents a single conductive medium with an uneven joint, as seen in Fig. 7.

As in case B, we can solve for the fields and contact resistance as a function of frequency. Doing so, we obtain $\overline{R_c}$ as a function of ω, as seen in Fig. 8.

At low frequencies, we again obtain a constant value for $\overline{R_c}$ that is equal to the DC contact resistance as in cases A and B. For very high frequencies ($\delta \ll d_2 - d_1 \ll d_1$), we obtain the frequency dependence described by (10), since the field profiles will look similar to those seen in Fig. 6. In this regime, the skin depth is much less than the "misalignment" ($d_2 - d_1$). It is then not surprising that the constriction resistance may far exceed the DC value, even though this misalignment is only 0.5% of the current channel width. For intermediate frequencies ($d_2 - d_1 \ll \delta \ll d_1$), we observe $\overline{R_c} \propto \omega$ from the numerical data (the dashed-dotted curves

Published under license by AIP Publishing.

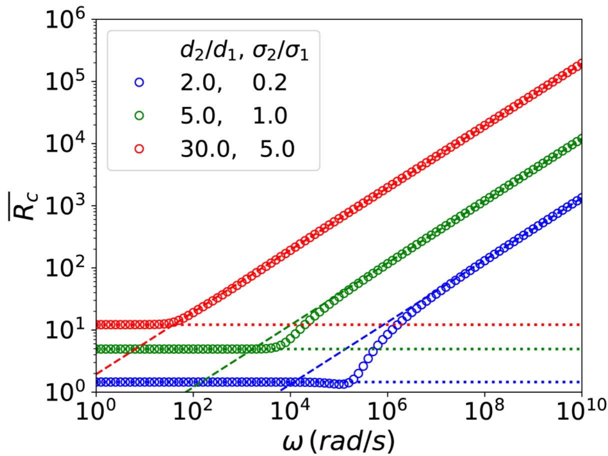

FIG. 5. $\overline{R_c}$ vs ω for various parameters. For all cases, $d_1 = 1$ mm and $\sigma_1 = 3.69 \times 10^7$ S/m. Dotted lines represent the DC contact resistance for each case. Dashed lines represent Eq. (10) for each case.

in Fig. 8). So far, we were unable to derive this frequency scaling even though for these intermediate frequencies, the current profile will look like Fig. 9. Note that the $\overline{R_c} \propto \omega$ scaling for the intermediate frequency regime is also suggested in the three curves in Fig. 5.

IV. CONCLUDING REMARKS

In this paper, we analyze the contact resistance between two Cartesian current channels of dissimilar materials and different widths, under the AC condition. Because of skin effects, even the bulk current densities are different from the DC case, leading to different expressions for the bulk resistances [Eq. (8)]. Assuming $\sigma \gg \epsilon\omega$, we can ignore currents flowing into conductor–vacuum interfaces, thereby simplifying the problem considerably. Three different cases were studied to obtain scaling laws for contact resistance as a function of frequency. For equal channel widths, $d_1 = d_2$, the low frequency limit always yields a zero contact resistance, which rises to a nonzero, constant value when the frequency is increased to a sufficiently high level. In this transition, negative contact resistance was observed and explained. In the general case, where $d_1 \neq d_2$, we obtain the DC contact resistance at low frequencies but find the normalized contact resistance $\overline{R_c} \propto \omega^{1/2}$ at very high frequencies. For a slightly uneven joint, $d_2 - d_1 \ll d_1$, $\sigma_1 = \sigma_2$, we obtain the DC contact resistance at low frequencies, $\overline{R_c} \propto \omega$ at intermediate frequencies, and $\overline{R_c} \propto \omega^{1/2}$ at high frequencies. The contact resistance is significantly more difficult to compute if we relax the assumption $\sigma \gg \epsilon\omega$.

When we are able to unambiguously define the AC contact resistance, by considering the ohmic power loss, the derived contact resistance may then be considered as a lumped circuit parameter. As of this writing, we were unable to find suitable and unambiguous definitions for the other lumped circuit parameters, the inductance and capacitance, for the current channel shown in Fig. 1, even under the assumption $\sigma \gg \epsilon\omega$.

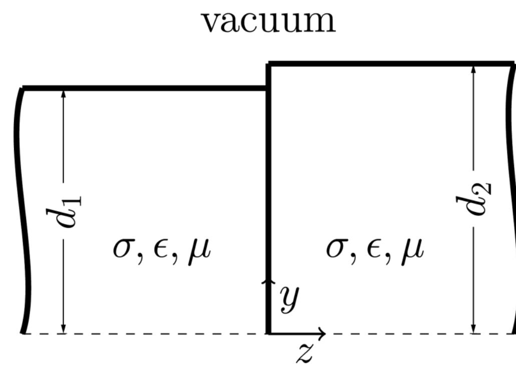

FIG. 7. An uneven join for a single material for case C.

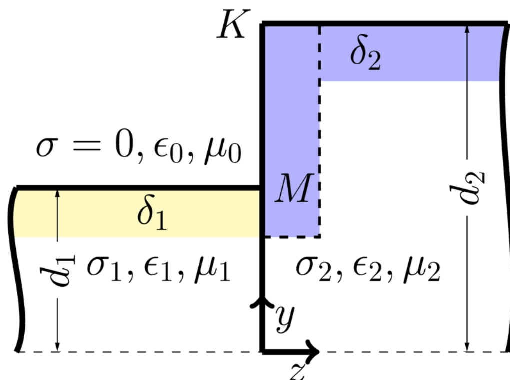

FIG. 6. Schematic drawing of the current profile near the channel surface in each conductor for high frequencies.

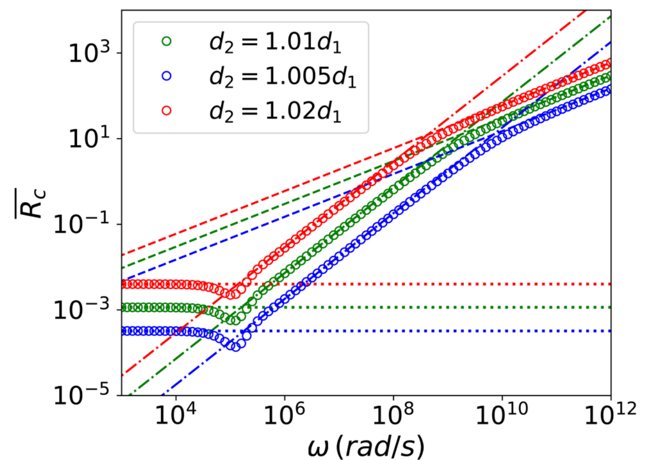

FIG. 8. $\overline{R_c}$ vs ω for an uneven joint. The dotted line represents the DC value for contact resistance, while the dashed line represents Eq. (10). The dashed-dotted line represents the fitted line $\overline{R_c} = A \times \omega$, where $A = 2.28 \left(\frac{d_2 - d_1}{\delta}\right)^2$ s. Here, $d_1 = 1$ mm and $\sigma_1 = 3.69 \times 10^7$ S/m.

Published under license by AIP Publishing.

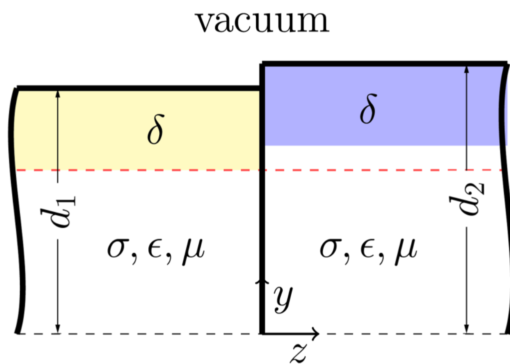

FIG. 9. The current profiled for $d_2 - d_1 \ll \delta \ll d_1$.

In Fig. 1, the point (y, z) = (d_1, 0) is a "triple point," the intersection of two different materials with vacuum.[34] We have examined the AC solutions at this triple point in some detail. This problem is of some practical and computational interest, but is beyond the scope of this paper.

Once more, if the conductivity σ is so small (like a semiconductor) or ω is so high (like submillimeter waves) that the simplifying assumption $\sigma \gg \epsilon\omega$ is no longer valid, then the contact resistance calculation will become very difficult. For one thing, the radiative loss, which is negligible in this paper, may need to be accounted for in the consideration of total power balance.

ACKNOWLEDGMENTS

We wish to thank Professor Peng Zhang for many useful discussions. This work was supported by Air Force Office of Scientific Research Award No. FA9550-18-1-0153, and by L3Harris Electron Devices Division.

APPENDIX A: FULL AC SOLUTION

First, let us consider the DC case [Fig. 10(a)].

To satisfy the boundary conditions (2a)–(2c), we include two fields in each conductor with the following form:

$$E_{z,A} = \sum_{n=1}^{\infty} A_n \cos\left(\frac{n\pi y}{d_1}\right) e^{\frac{n\pi z}{d_1}},\quad E_{y,A} = \sum_{n=1}^{\infty} -A_n \sin\left(\frac{n\pi y}{d_1}\right) e^{\frac{n\pi z}{d_1}}, \tag{A1a}$$

in the left conductor and

$$E_{z,B} = \sum_{n=1}^{\infty} B_n \cos\left(\frac{n\pi y}{d_2}\right) e^{-\frac{n\pi z}{d_2}},\quad E_{y,B} = \sum_{n=1}^{\infty} B_n \sin\left(\frac{n\pi y}{d_2}\right) e^{-\frac{n\pi z}{d_2}}, \tag{A1b}$$

in the right conductor. These fields are chosen to enforce symmetry around the $y = 0$ plane, as well as to ensure that (2d) and (2e) are satisfied. Field "A" is meant to satisfy (2b) and is, therefore, a Fourier representation over ($z = 0,\ y \in [0, d_1]$), while field "B" is meant to satisfy (2a) and (2c) and is, therefore, a Fourier representation over ($z = 0,\ y \in [0, d_2]$). In Fig. 10(a), these regions can be seen. Next, we truncate the Fourier series for each field to N terms, since convergence was proven in Ref. 24. This allows us to use (2a)–(2c) to obtain a $2N \times 2N$ matrix that can be inverted to yield A_n and B_n, and therefore the fields everywhere.

Moving on to the AC case, the boundary conditions now have the following form [Fig. 10(b)]:

$$E_{y,1} = E_{y,2},\qquad z = 0,\qquad |y| < d_1, \tag{A2a}$$

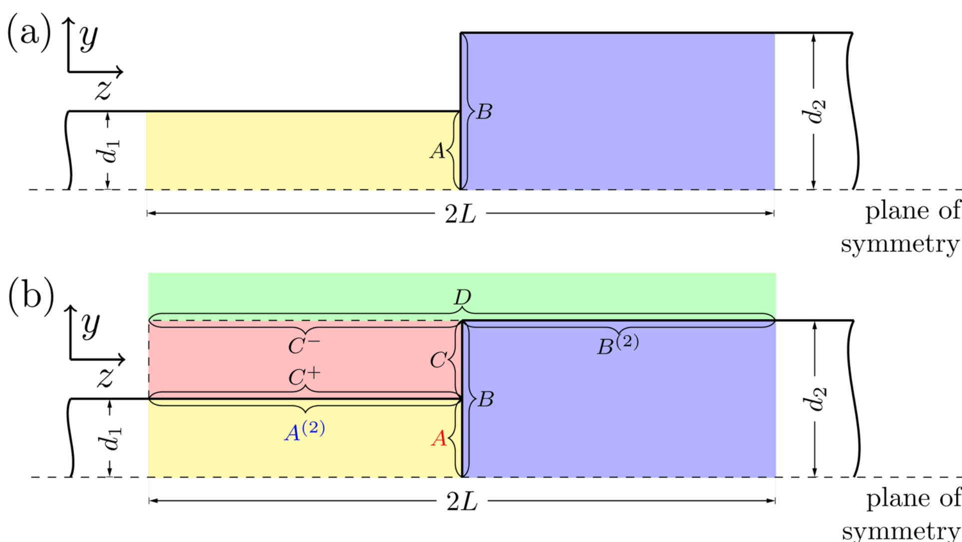

FIG. 10. The colored regions, which are considered, as well as the boundary terms for the DC case (a) and the AC case (b).

Published under license by AIP Publishing.

$$(\sigma_2 - i\omega\epsilon_2)E_{z,2} = \begin{cases} (\sigma_1 - i\omega\epsilon_1)E_{z,1}, & |y| < d_1 \\ -i\omega\epsilon_0 E_{z,3}, & d_1 < |y| < d_2 \end{cases}, \tag{A2b}$$

$$E_{z,1} = E_{z,3}, \quad |y| = d_1, \quad z < 0, \tag{A2c}$$

$$(\sigma_1 - i\omega\epsilon_1)E_{y,1} = (\sigma_3 - i\omega\epsilon_3)E_{y,3}, \quad |y| = d_1, \quad z < 0, \tag{A2d}$$

$$E_{y,2} = E_{y,3}, \quad z = 0, \quad d_1 < |y| < d_2, \tag{A2e}$$

$$E_{y,3} = E_{y,4}, \quad |y| = d_2, \quad z < 0, \tag{A2f}$$

$$(\sigma_2 - i\omega\epsilon_2)E_{y,2} = -i\omega\epsilon_0 E_{y,4}, \tag{A2g}$$

$$E_{z,4} = \begin{cases} E_{z,3} \; z < 0 \\ E_{z,2}, \; z > 0 \end{cases}, \quad |y| = d_2, \tag{A2h}$$

where E_3 corresponds to fields within ($z \in [-L, 0]$, $y \in [d_1, d_2]$) [red region in Fig. 10(b)] and E_4 to fields within ($z \in [-L, L]$, $y \in [d_2, \infty]$) [green region in Fig. 10(b)]. To satisfy all of the above, we need to include a field that is a Fourier transform for each boundary condition. All the regions that have a Fourier transform over them can be seen in Fig. 10(b). The resulting total $E_{z,1}$ in the conductor to the left is

$$\begin{aligned} E_{1,z} =& \frac{I_0\kappa_2}{2W\sigma_2}\frac{\cos(\kappa_2 y)}{\sin(\kappa_2 d_2)} \quad \text{(bulk solution)} \\ &+ \sum_{n=1}^{\infty} A_n \cos\left(\frac{n\pi y}{d_1}\right) e^{z\sqrt{\left(\frac{n\pi}{d_1}\right)^2 - \kappa_1^2}} \quad \text{[meant to satisfy (A2a)]} \\ &+ \sum_{n=1}^{\infty} A_n^{(2)} \sin\left(\frac{(2n-1)\pi z}{2L}\right) e^{y\sqrt{\left(\frac{(2n-1)\pi}{2L}\right)^2 - \kappa_1^2}} \\ &\text{[meant to satisfy (A2d)].} \end{aligned}$$

Numerically, the last infinite sum is very small for all cases studied in this paper. Truncating all series to N once more and using Eqs. (A2a)–(A2h) and all of the fields that were included, we can obtain a $8N \times 8N$ matrix which can again be solved numerically. Doing so, however, requires 16 times more memory and ~64 times more time than the DC case with the same N. For $\sigma \gg \omega\epsilon$, Eqs. (A2a)–(A2h) turn into (2a)–(2e) and we only need fields "A" and "B" again and then use the matching techniques given in Ref. 24. Note that the "A" and "B" solutions satisfy the Laplace (Helmholtz) equation for the DC (AC) case. Comparing the full solution utilizing all eight Fourier fields to the simplified solution for $\sigma \geq 3.69 \times 10^5$ and $\omega/2\pi \leq 10$ THz, we obtain contact resistances within 0.000042% of each other, for a few test cases. For semiconductors, the full solution would need to be used, but L needs to be much larger consequently and a larger N needs to be used for proper accuracy.

APPENDIX B: BULK SOLUTIONS FOR THE AC CASE

Solving Maxwell's equations under the AC condition in a conductor yields fields that are proportional to

$$\begin{aligned} F(z, y) &= e^{ik_z z} e^{ik_y y}, \\ k_z^2 + k_y^2 &= \mu\epsilon\omega^2 + i\omega\mu\sigma. \end{aligned} \tag{B1}$$

For the bulk currents in each conductor, we have $k_z = 0$ and $E_y = 0$. Furthermore, fields need to be symmetric around the $y = 0$ axis. This means that the only fields in each conductor are

$$\begin{aligned} E_{z,1,b} &= E_1 \cos(\kappa_1 y), \quad |y| < d_1, \\ E_{z,2,b} &= E_2 \cos(\kappa_2 y), \quad |y| < d_2, \\ \kappa_1^2 &= \mu_1\epsilon_1\omega^2 + i\omega\mu_1\sigma_1, \\ \kappa_2^2 &= \mu_2\epsilon_2\omega^2 + i\omega\mu_2\sigma_2, \end{aligned} \tag{B2}$$

where E_1 and E_2 are complex constants. To find their respecting values, we solve

$$\begin{aligned} W\int_{-d_1}^{d_1} \sigma_1 E_{z,1,b}\, dy &= I_0, \\ W\int_{-d_2}^{d_2} \sigma_2 E_{z,2,b}\, dy &= I_0, \end{aligned} \tag{B3}$$

to obtain

$$\begin{aligned} E_1 &= \frac{I_0\kappa_1}{2W\sigma_1}\frac{1}{\sin(\kappa_1 d_1)}, \\ E_2 &= \frac{I_0\kappa_2}{2W\sigma_2}\frac{1}{\sin(\kappa_2 d_2)}, \end{aligned} \tag{B4}$$

which can be used with (B2) to yield Eq. (5) of the main text. To obtain the bulk resistance, we first consider $\sigma \gg \omega\epsilon$ so that (6) gives

$$\begin{aligned} \kappa_1 &\approx \frac{1+i}{\delta_1}, \\ \kappa_2 &\approx \frac{1+i}{\delta_2}. \end{aligned} \tag{B5}$$

The average power dissipated in each conductor will be

$$P = \sigma\int_V \left[\frac{|\boldsymbol{E}^2|}{2}\right] dV. \tag{B6}$$

Using this, we now obtain the time averaged power per unit length for the left conductor

$$\frac{dP_1}{dl} = \frac{I_0^2}{4W\sigma_1\delta_1^2}\int_{-d_1}^{d_1} \frac{\cos\left(\frac{1+i}{\delta_1}y\right)\cos\left(\frac{1-i}{\delta_1}y\right)}{\sin\left(\frac{i+1}{\delta_1}d_1\right)\sin\left(\frac{i-1}{\delta_1}d_1\right)}\, dy.$$

Published under license by AIP Publishing.

Using

$$\sin((1+i)x)\sin((1-i)x) = \frac{1}{2}(\cosh(2x) - \cos(2x)),$$

$$\cos((1+i)x)\cos((1-i)x) = \frac{1}{2}(\cosh(2x) + \cos(2x)),$$

we obtain

$$\frac{dP_1}{dl} = \frac{I_0^2}{2W\sigma_1\delta_1}\frac{\sinh\left(\frac{2d_1}{\delta_1}\right) + \sin\left(\frac{2d_1}{\delta_1}\right)}{\cosh\left(\frac{2d_1}{\delta_1}\right) - \cos\left(\frac{2d_1}{\delta_1}\right)}.$$

Equating this to $\frac{RI_0^2}{2L}$ because of (3), we can obtain

$$R_{b1} = \frac{L}{2W\sigma_1\delta_1}\frac{\sinh\left(\frac{2d_1}{\delta_1}\right) + \sin\left(\frac{2d_1}{\delta_1}\right)}{\cosh\left(\frac{2d_1}{\delta_1}\right) - \cos\left(\frac{2d_1}{\delta_1}\right)}. \tag{B7}$$

Similarly, for the second conductor one can obtain

$$R_{b2} = \frac{L}{2W\sigma_2\delta_2}\frac{\sinh\left(\frac{2d_2}{\delta_2}\right) + \sin\left(\frac{2d_2}{\delta_2}\right)}{\cosh\left(\frac{2d_2}{\delta_2}\right) - \cos\left(\frac{2d_2}{\delta_2}\right)}. \tag{B8}$$

Equations (B7) and (B8) are Eq. (8) from the text.

APPENDIX C: $\overline{R_c} \propto \omega^{1/2}$ DERIVATION

As ω increases, δ_1 and δ_2 will decrease. This means that at sufficiently high frequencies, the following will be true:

$$\begin{aligned} \delta_1 &\ll d_1, \\ \delta_2 &\ll d_2, \\ \delta_2 &\ll d_2 - d_1. \end{aligned} \tag{C1}$$

When the above are true, the current will be confined to the edges of the conductors. Such a current flow can be seen in Fig. 6 of the main text. The horizontal currents in each conductor are the bulk currents, which do not contribute to the contact resistance. The only remaining currents to consider are the vertical current between points M and K as well as current perturbations to attain transitions that satisfy all relevant boundary conditions. The latter perturbations, however, will be confined to areas that are in order of δ_1^2 or δ_2^2, whereas the vertical current will occupy an area in the order of $(d_2 - d_1)\delta_2$. From Eq. (C1), $\delta_2^2 \ll (d_2 - d_1)\delta_2$. Furthermore,

$$\frac{\delta_1^2}{(d_2 - d_1)\delta_2} \propto \omega^{-\frac{1}{2}}. \tag{C2}$$

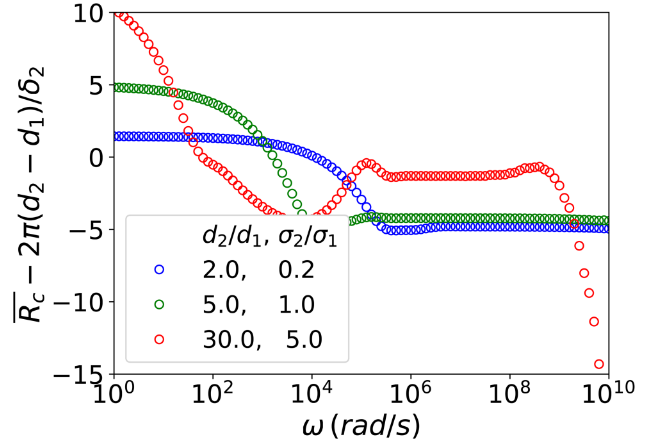

FIG. 11. Residual normalized contact resistance after subtracting Eq. (C5).

For sufficiently high frequencies, we can also, therefore, assume $\delta_1^2 \ll (d_2 - d_1)\delta_2$. Because of the above, we can assume that the contact resistance will primarily arise from the vertical current between points M and K, which we shall explicitly show toward the end of this Appendix. The current distribution in this area is approximately

$$J = \frac{I_0}{W\delta_2}e^{-\frac{z}{\delta_2}}, \tag{C3}$$

which will dissipate a total power of

$$P = \int_a^b dy \int_0^W dx \int_0^\infty \frac{J^2}{\sigma_2}\, dz = \frac{(b-a)I_0^2}{2W\delta_2\sigma_2}. \tag{C4}$$

Equating the above with $\frac{R_c I_0^2}{2}$ as per (3) and normalizing using (9), we obtain

$$\overline{R_c} = 2\pi\frac{b-a}{\delta_2} \propto \omega^{\frac{1}{2}}, \tag{C5}$$

which is Eq. (10) in the main text. Subtracting Eq. (C5) from the data on Fig. 5 yields Fig. 11. This gives the remaining constriction resistance near M and near K, which appears to attain constant values for sufficiently high frequencies. Note that the significant drop in constriction resistance for $d_2/d_1 = 30$ and $\sigma_2/\sigma_1 = 5$ are numerical artifacts: changing the number of terms that are kept in the Fourier series changes the onset of this effect. This is because the skin depth becomes too small compared to the thickness of the materials (for $\omega = 10^8$ rad/s, $\delta_2/d_2 = 3 \times 10^{-4}$). A comparison of Fig. 5 and Fig. 11 demonstrates that constriction effects are insignificant compared to the vertical skin current that flows between the points M and K. The feature that the constriction resistance approaching a constant value at high frequencies was revealed in and also commented on in Fig. 3. It was also explored in Ref. 25 and in p. 91 of Ref. 1.

Published under license by AIP Publishing.

REFERENCES

[1] R. S. Timsit, "Electrical contact resistance: Fundamental principles," in *Electrical Contacts Principles and Applications*, edited by P. G. Slade (Marcel Dekker, New York, 1999), p. 1.
[2] R. Holm, *Electric Contact*, 4th ed. (Springer-Verlag, Berlin, 1967).
[3] "Review of federal programs for wire systems safety," Final Report (National Science and Technology Council, Washington, DC, November, 2000).
[4] M. Gomez, J. C. Zier, R. M. Gilgenbach, D. M. French, W. Tang, and Y. Y. Lau, "Effect of soft metal gasket contacts on contact resistance, energy deposition, and plasma expansion profile in a wire array Z-pinch," Rev. Sci. Instrum. **79**, 093512 (2008).
[5] M. D. Haworth, G. Baca, J. Benford, T. Englert, K. Hackett, K. J. Hendricks, D. Henley, M. LaCour, R. W. Lemke, D. Price, D. Ralph, M. Sena, D. Shiffler, and T. A. Spencer, "Significant pulse-lengthening in a multigigawatt magnetically insulated transmission line oscillator," IEEE Trans. Plasma Sci. **26**(3), 312–319 (1998).
[6] P. Bruzzone, B. Stepanov, R. Dettwiler, and F. Staehli, IEEE Trans. Appl. Supercond. **17**, 1378 (2007); A. Nijhuis, Y. Ilyin, W. Abbas, B. ten Haken, and H. H. J. ten Kate, Cryogenics **44**, 319 (2004).
[7] H. Gelinck, T. C. T. Geuns, and D. M. de Leeuw, Appl. Phys. Lett. **77**, 1487 (2000).
[8] W. J. Greig, *Integrated Circuit Packaging, Assembly, and Interconnections* (Springer, New York, 2007).
[9] L. Carbonero, G. Morin, and B. Cabon, IEEE Trans. Microw. Theory Tech. **43**, 2786 (1995); H. Klauk, G. Schmid, W. Radlik, W. Weber, L. Zhou, C. D. Sheraw, J. A. Nichols, and T. N. Jackson, Solid State Electron. **47**, 297 (2003).
[10] S. B. Fairchild, J. Boeckl, T. C. Back, J. B. Ferguson, H. Koerner, P. T. Murray, B. Maruyama, M. A. Lange, M. M. Cahay, N. Behabtu, C. C. Young, M. Pasquali, N. P. Lockwood, K. L. Averett, G. Gruen, and D. E. Tsentalovich, "Morphology dependent field emission of acid-spun carbon nanotube fibers," Nanotechnology **26**(10), 105706 (2015); R. H. Baughman, A. A. Zakhidov, and W. A. de Heer, "Carbon nanotubes—The route toward applications," Science **297**, 787 (2002).
[11] D. Shiffler, T. K. Statum, T. W. Hussey, O. Zhou, and P. Mardahl, "High power microwave sources," in *Modern Microwave and Millimeter Wave Power Electronics* (IEEE, Piscataway, NJ, 2005), p. 691; W. Tang, D. Shiffler, K. Golby, M. LaCour, and T. Knowles, "Experimental study of electron field screening by the proximity of two carbon fiber cathodes," J. Vac. Sci. Technol. B **30**, 061803 (2012).
[12] W. Wu, S. Krishnan, T. Yamada, X. Sun, P. Wilhite, R. Wu, K. Li, and C. Y. Yang, Appl. Phys. Lett. **94**, 163113 (2009); Z. Yao, C. L. Kane, and C. Dekker, Phys. Rev. Lett. **84**, 2941 (2000); D. Mann, A. Javey, J. Kong, Q. Wang, and H. Dai, Nano Lett. **3**, 1541 (2003); A. Mikrajuddina, F. G. Shib, H. K. Kimb, and K. Okuyama, "Size-dependent electrical constriction resistance for contacts of arbitrary size: From Sharvin to Holm limits," Mater. Sci. Semicond. Process. **2**, 321–327 (1999).
[13] K. L. Jensen, *Introduction to the Physics of Electron Emission* (Wiley, Hoboken, NJ, 2017); K. L. Jensen, D. A. Shiffler, I. M. Rittersdorf, J. L. Lebowitz, J. R. Harris, Y. Y. Lau, J. J. Petillo, W. Tang, and J. W. Luginsland, "Discrete space charge affected field emission: Flat and hemisphere emitters," J. Appl. Phys. **117**, 194902 (2015).
[14] R. Timsit, in *Proceedings of the 54th IEEE Holm Conference on Electrical Contacts* (IEEE, 2008), pp. 332–336; M. B. Read, J. H. Lang, A. H. Slocum, and R. Martens, in *Proceedings of the 55th IEEE Holm Conference on Electrical Contacts* (IEEE, 2009), pp. 303–309; G. Norberg, S. Dejanovic, and H. Hesselbom, IEEE Trans. Compon. Packag. Technol. **29**, 371 (2006); K. Nagashio, T. Nishimura, K. Kita, and A. Toriumi, "Contact resistivity and current flow path at metal/graphene contact," Appl. Phys. Lett. **97**, 143514 (2010).
[15] H. Kam, E. Alon, and T.-J.K. Liu, in *Electron Devices Meeting (IEDM), 2010 IEEE International* (IEEE, 2010), pp. 16.4.1–16.4.4.
[16] M. B. Read, J. H. Lang, A. H. Slocum, and R. Martens, "Contact resistance in flat thin films," in *Proceedings of the 55th IEEE Holm Conference on Electrical Contacts* (IEEE, 2009), pp. 303–309.
[17] S. Datta, *Quantum Transport Atom to Transistor* (Cambridge University Press, New York, 2005).
[18] P. Zhang, Q. Gu, Y. Y. Lau, and Y. Fainman, "Constriction resistance and current crowding in electrically pumped semiconductor nanolasers with the presence of undercut and sidewall tilt," IEEE J. Quantum Electron. **52**, 2000207 (2016).
[19] Q. Gu and Y. Fainman, *Semiconductor Nanolasers* (Cambridge University Press, 2017).
[20] P. Zhang and Y. Y. Lau, "Ultrafast and nanoscale diodes," J. Plasma Phys. **82**, 595820505 (2016).
[21] P. Zhang, S. B. Fairchild, T. C. Back, and Y. Luo, "Field emission from carbon nanotube fibers in varying anode-cathode gap with the consideration of contact resistance," AIP Adv. **7**, 125203 (2017).
[22] S. Benerjee, J. W. Luginsland, and P. Zhang, "A two dimensional tunneling resistance transmission line model for nanoscale parallel electrical contacts," Sci. Rep. **9**, 14484 (2019); S. Benerjee and P. Zhang, "A generalized self-consistent model for quantum tunneling current in dissimilar metal-insulator-metal junction," AIP Adv. **9**, 085302 (2019).
[23] Y. Y. Lau and W. Tang, "A higher dimensional theory of electrical contact resistance," J. Appl. Phys. **105**, 124902 (2009).
[24] P. Zhang and Y. Y. Lau, "Scaling laws for electrical contact resistance with dissimilar materials," J. Appl. Phys. **108**, 044914 (2010).
[25] P. Zhang, Y. Y. Lau, and R. S. Timsit, "On the spreading resistance of thin film contacts," IEEE Trans. Electron Devices **59**, 1936 (2012); P. Zhang, Doctoral dissertation, University of Michigan, 2012.
[26] P. Zhang, D. M. H. Hung, and Y. Y. Lau, "Current flow in a 3-terminal thin film contact with dissimilar materials and general geometric aspect ratios," J. Phys. D Appl. Phys. **46**, 065502 (2013).
[27] P. Zhang and Y. Y. Lau, "Constriction resistance and current crowding in vertical thin film contact," IEEE J. Electron Device Soc. **1**, 83 (2013).
[28] P. Zhang and Y. Y. Lau, "An exact field solution of contact resistance and comparison with the transmission line model," Appl. Phys. Lett. **104**, 204102 (2014).
[29] P. Zhang, Y. Y. Lau, and R. M. Gilgenbach, "Analysis of current crowding in thin film contacts from exact field solutions," J. Phys. D Appl. Phys. **48**, 475501 (2015).
[30] R. S. Timsit, "Electrical contact resistance: Properties of stationary interfaces," IEEE Trans. Compon. Packag. Technol. **22**(1), 85–98 (1999).
[31] R. S. Timsit, "Constriction resistance of thin-film contacts," IEEE Trans. Compon. Packag. Technol. **33**(3), 636–642 (2010).
[32] R. S. Timsit and A. Luttgen, "Temperature distribution in an ohmic-heated electrical contact at high signal frequencies," Appl. Phys. Lett. **108**, 121603 (2016).
[33] W. Tang, Y. Y. Lau, and R. M. Gilgenbach, "Lumped circuit elements, statistical analysis, and radio frequency properties of electrical contact," J. Appl. Phys. **106**, 084904 (2009).
[34] N. M. Jordan, Y. Y. Lau, D. M. French, R. M. Gilgenbach, and P. Pengvanich, "Electric field and electron orbits near a triple point," J. Appl. Phys. **102**, 033301 (2007).

Published under license by AIP Publishing.